Study on the tissue clearing process using different agents by Mueller matrix microscope

QIAOLIN XIE,[1,2,9] NAN ZENG,[1,9,*] YU HUANG,[1,2] VALERY V. TUCHIN,[5,6,7,8] AND HUI MA[1,3,4,10]

[1]Key Laboratory for Minimal Invasive Medical Technologies, 2279 Lishui Street, Shenzhen 518055, China
[2]Tsinghua University, Department of Biomedical Engineering, 1 Tsinghua Yuan, Beijing 100084, China
[3]Tsinghua University, Department of Physics, 1 Tsinghua Yuan, Beijing 100084, China
[4]Center for Precision Medicine and Healthcare, Tsinghua-Berkeley Shenzhen Institute, Shenzhen, 518071, China
[5]Saratov State University, 83 Astrakhanskaya Street, Saratov 410012, Russia
[6]Tomsk State University, 36 Lenin Avenue, Tomsk 634050, Russia
[7]Institute of Precision Mechanics and Control of RAS, 24 Rabochaya Street, Saratov 410028, Russia
[8]Bach Institute of Biochemistry, Research Center of Biotechnology of the Russian Academy of Sciences, 33-2 Leninsky prospect, Moscow 119071, Russia
[9]These authors contributed equally to this work.
[10]mahui@tsinghua.edu.cn
[*]zengnan@sz.tsinghua.edu.cn

Abstract: In this paper, we monitor the in vitro tissue clearing process of mouse dorsal skin immersed into two types of agents using Mueller matrix microscope. By Mueller matrix polar decomposition, we can see that the major difference between polarization changes due to two kinds of agents is the opposite trend of phase retardance with clearing. For the insight of the connection between different agents with the microstructural and optical changes of cleared tissues, we establish various models to mimic the dynamic process of microphysical features of tissues with clearing time. The mechanisms considered include refractive index matching, collagen shrinkage, more orderly fibers and birefringence variation. We compare the experimental results with simulations based on a single mechanism model and a combined model, respectively, which confirms that an individual possible mechanism cannot explain the polarization phenomena due to clearing. Also by simulations of various clearing models involving two possible mechanisms, we can speculate that formamide and saturated sucrose as agents have respective impacts on tissue features and then cause different polarization changes with clearing. Specifically, collagen shrinkage plus birefringence reduction can better explain the tissue cleared by formamide, and refractive index match plus increased birefringence model is likely to be a proper description of tissue cleared by sucrose. Both simulations and experiments also validate the potential of Mueller matrix microscope as a good tool to understand the interaction between clearing agents and tissues.

1. Introduction

Tissues contain a mix of components of small size with different refractive indexes (RIs), the interactions of light with these heterogeneous components lead to a lack of transparency. Tissue clearing methods make tissues transparent by homogenize the RI by removing, replacing and modifying some of its components [1]. Due to its contribution to penetration depth and then imaging resolution and contrast, tissue optical clearing (TOC) techniques are becoming more and more prominent in biomedical applications [2–4]. Related research interests include ex-vivo and in-vivo experiments, potential clearing agents and pretreatment mode, molecular dynamics simulations and new applications [5–9]. Many optical imaging methods such as optical coherence tomography (OCT) [10,11], laser speckle contrast imaging

(LSCI) [12], 3D-confocal microscopy [13], polarized microscopy [14], and multiphoton imaging [15] can be combined with TOC. These advanced optical methods promote studies on the molecular and microstructure and function of tissues in vivo or in vitro also can be used to evaluate the efficacy of TOC.

Usually, simple immersion is passive clearing method by place the thin tissue into high refractive index solutions [1]. There are many OCAs which been used as this purpose, such as sucrose [16], fructose [17], glycerol [18], formamide [19], and 2,2'-thiodiethanol (TDE) [20]. The OC efficacy depends on the type and concentration of OCAs as well as on its treatment time [21]. Besides chemical enhancers, physical methods have also been used to improve OC, such as microdermabrasion [22], laser irradiation of skin surface [23], iontophoresis [24], ultrasound [25] and photothermal and mechanical microperforation [26].

There are several possible mechanisms about the explanations of OC process [21]. The first and the most common explanation is refractive index matching. The second common explanation is collagen shrinkage. There are some corresponding experiments showing that sample's thickness changes significantly with clearing [27]. The third common explanation is more orderly collagen, which implies that scatterers' near-order spatial correlation is enhanced, and thus the lateral scattering is minimized or even eliminated [28].

Polarization imaging techniques are sensitive to microstructural changes in tissues, and can therefore be regarded as potential and label-free tools for physiological process monitoring and pathological diagnosis. Recently, polarization techniques are attracting more and more attention in biomedicine [29–33]. As a comprehensive description of polarization characteristics of scattering samples, Mueller matrix polarimetry has demonstrated promising potential in abnormal tissues detection for both backward scattering imaging of bulk tissue samples and transmission imaging of thin tissue slices [34–36]. In our previous research, we studied the influence of TOC on tissue polarization imaging [37,38], and give some preliminary explanations using our Monte Carlo simulations [39] combined with our anisotropic tissue model [40]. Also by Mueller matrix polar decomposition method, we show a semi-quantitative description on the polarization optical change due to tissue clearing.

In this paper, we focus on the tissue clearing process using two types of OCAS and try to explain the difference of dynamic microstructural change of cleared tissue and understand how these two OCAS make tissues clear respectively. Collagen fibers are typical anisotropic tissues and can generate obvious polarization optical phenomenon, and there are studies showing that hydroxyl molecules in OCAs will interact with collagen and affect the clearing results [10]. So we use skin rich in collagen fibers as the research object, and observe the polarization features by Mueller matrix imaging and MMPD method combined with Monte Carlo simulation of various tissue clearing mechanisms.

2. Method and experiment setup

2.1 Sample and OCAs

Our experimental tissue samples are taken from seven-week-old nude mice from Guangdong Medical Lab Animal Center. They were fed under specific pathogen-free conditions. After mice being sacrificed, a 3x3 cm skin with a thickness of 1mm was cut from mice's back. Then, we divided the skin into 9 small pieces on average, with each piece 1x1 cm. Subsequently, these pieces of skin are immersed in two different types of OCAs and measured by polarized forward microscope to obtain their Mueller matrix images.

Polarization status is an effective way to study the microscopic changes in tissues and is especially sensitive to those optical anisotropic features, such as birefringence or fibrous microstructures. Collagen fibers are the main components of dermis, and show an apparent anisotropic scattering capability in our previous research work [38,41]. There are studies that the hydroxyl molecule in OCAs will interact with collagen and cause various possible microcosmic changes of fiber content and arrangement. We select formamide and saturated sucrose as our agents, because the molecular structure of the latter does contain hydroxyl

groups and the former does not. This paper not only study what happens when the tissue is becoming transparent gradually, but also investigate the influence of different agents with or without hydroxyl molecule on tissue clearing. Figure 1 shows the molecular structure of these two agent: formamide and saturated sucrose. Under the temperature of 20°C, formamide's refractive index is 1.447 and 100% saturated sucrose's refractive index is 1.5476.
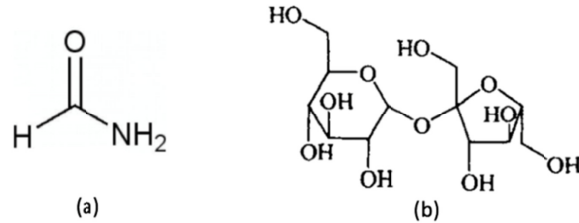

Fig. 1. The molecular structure of formamide (a) and saturated sucrose (b).

2.2 Experiment setup

The Mueller matrix microscope we used is a forward scattering polarized microscope [31], as shown in Fig. 2. The light source is a LED with the wavelength of 632.8 nm. The incident polarization state of the collimated light is controlled by a linear polarizer P1 with a polarization extinction of 500:1 and a rotatable quarter-wave plate. When the light illuminates the tissue sample, the polarization state of forward scattered photons is analyzed by the second quarter-wave plate and the second linear polarizer P2 at the imaging end. Finally, the photons are recorded by a QIClickTM CCD camera (QImaging,12-bit 1394 x 1040 pixels).
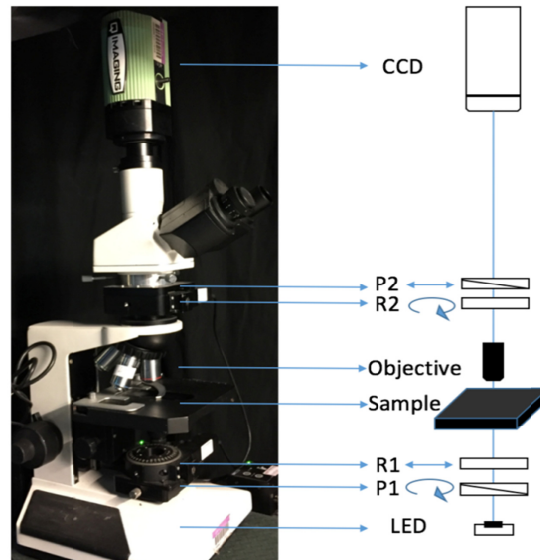

Fig. 2. Mueller matrix microscope.

2.3 Monte Carlo simulations

In our previous research work [36–38], Monte Carlo simulation and sphere-cylinder birefringence model (SCBM) have been verified to be very helpful to recognize and differentiate the tissue microstructure and optical properties. To understand the possible mechanisms of tissue clearing process and find out the major difference from clearing effects by two different agents, we will mimic the dynamic process of tissue clearing based on our

polarization scattering calculation program and SCBM tissue model and compare them with experimental results in the following section.

In sphere-cylinder birefringence model (SCBM), as shown in Fig. 3, sphere scatterers represent cells and other isotropic microstructures, such as nuclei and other organelles. Cylindrical scatterers represent fibrous microstructures like collagen fibers in skin tissue. Birefringence is introduced in our tissue model considering the optical anisotropy at molecular level. By combination of Monte Carlo simulation and SCBM, we can mimic various tissue types and simulate the transmission and scattering of polarized light in biological tissues.

In our simulation program, variable parameters for scatterers include scattering coefficient, diameter of the spheres and cylinders, the mean value and standard deviation of the orientation distribution function for the cylinders. For the ambient medium, variable parameters include the refractive index, the absorption coefficient, the optical activity coefficient, and the value and orientation of birefringence.
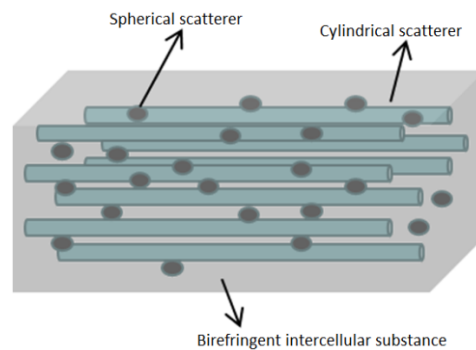

Fig. 3. Sphere-cylinder birefringence model (SCBM).

The initial state of skin tissue before clearing can be set as follows [42,43]: the tissue thickness is 1mm; the diameter of spheres and cylinders are 0.2μm and 1.5μm, respectively; the scattering coefficient of spheres and cylinders are 20 cm^{-1} and 180cm^{-1}; the refractive indices of the interstitial medium and the scatterers (including spheres and cylinders) are 1.35 and 1.43, respectively; the cylinders are along the x-axis direction with a FWHM of 18 degree in the orientation distribution considering collagen fibers packed in bundles and arranged in a lamellae structure; the birefringence value is 3e-5 and its optical axis is along the x-axis; the wavelength of the incident light is 633nm and the simulated photon number is 10e7.

To mimic tissue optical clearing process by different agents, we consider various dynamic models corresponding to several possible clearing mechanisms including refractive index match, tissue shrinkage by dehydration, fluctuation of birefringence effect in intercellular substance and ordering of fiber arrangement. In the following studies, we will start with the simulations based on one single mechanism and compare them respectively with experiments, and then we will observe whether the parallel simulations based on two major mechanisms can explain the experimental phenomena better.

3. Results

3.1 Experimental results of tissue clearing with different agents

Simple immersion is a very convenient and useful way to make tissue transparent. In Fig. 4 the skin samples are put on a 1951 United States Air Force (USAF) resolution test target before and after treatment with two kinds of agents: formamide and saturated sucrose. White-light images make clear that these two OCAs we choose have a rapid and apparent effect to

make tissue transparent within 20 min. At the beginning, the mouse skin sample can almost cover the pattern of the resolving power test target completely. After 10-min and 20-min treatments, mouse skin become more and more transparent in both Figs. 4(a) and 4(b), thus the pattern of the resolving power test target can be identified step by step.
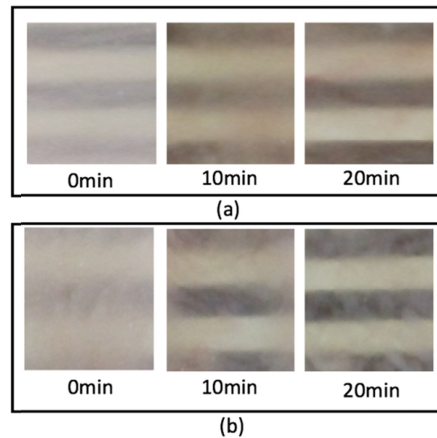

Fig. 4. White-light images of in vitro rat skin before and after clearing by formamide (a) and saturated sucrose (b). The background is small region of 1951 USAF target.

At different time points during clearing, we record 4x4 Mueller matrix images of the cleared mouse's skin. To better understand the polarization-dependent physical processes with clearing, we employ the Mueller matrix polar decomposition method (MMPD) to obtain the depolarization parameter Δ and retardation parameter δ, where the diattenuation parameter by MMPD is approximate zero and has no change with clearing. The size of area detected by CCD is a square area about 2 mm × 2 mm.

Firstly, to achieve a comprehensive observation of tissue's polarization state with clearing process, Mueller matrix images using formamide and saturated sucrose as OCAs are shown in Fig. 5. Here the m_{11} representing the scattering intensity is normalized by its max value and the other 15 Mueller elements also has been normalized by the maximum intensity. From the figure, we can find out the roughly polarization changes due to tissue clearing. The four diagonal elements, including intensity element m11, and depolarization correlated elements: m22, m33 and m44, are increasing apparently, which fits well the improved light penetration and suppressed scattering phenomena by OCAs. Non-diagonal elements have relatively small values and changes, however, their trends and differences often provide more detailed information on tissue microstructure and optical properties. When using formamide as agent, the values of m13, m14, m31, m34, m41 and m43 are changed, but when using saturated sucrose as agent, the non-diagonal elements affected by clearing are m23, m24, m32, m34, m42, m43. The most interesting difference using these two types of OCAS is the opposite trends of m34 and m43, where the formamide agent decreases their absolute values and the saturated sucrose increases their absolute values. According to our research works on Mueller matrix characterization, these two elements can be closed related with tissue anisotropy, especially from intercellular birefringence effect. Except for m34 and m43, the fluctuation of other non-diagonal elements maybe are connected with the arrangement of fibrous structures, scatterer size or optical rotation effect.
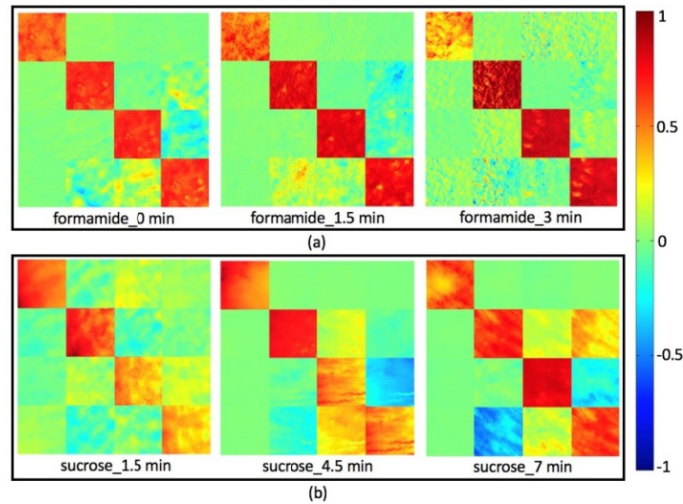
Fig. 5. Pseudo-color images of the Mueller matrix elements at three time points during clearing process using formamide(a) and saturated sucrose(b) as OCAs.

Figures 6 and 7 show the tissue images and the values of depolarization and phase retardance with clearing time. In Fig. 6, to analyze MMPD parameters quantitatively, we randomly choose 15 square areas with the size of 35.5μm × 35.5μm in the detected images, then we calculate the average values and standard deviations of parameters Δ and δ, respectively. Here the unit of phase retardance is phase delay angle not radian.

When using formamide as optical clearing agent, both the depolarization parameter and the retardation parameter decrease dramatically. However, when using saturated sucrose as agent, by the same experiment setup, the depolarization parameter is also decreased apparently, but the phase retardance increases with the oscillatory behavior. It looks like that it is a key factor to explain the opposite tendency of retardance with clearing due to different agents.
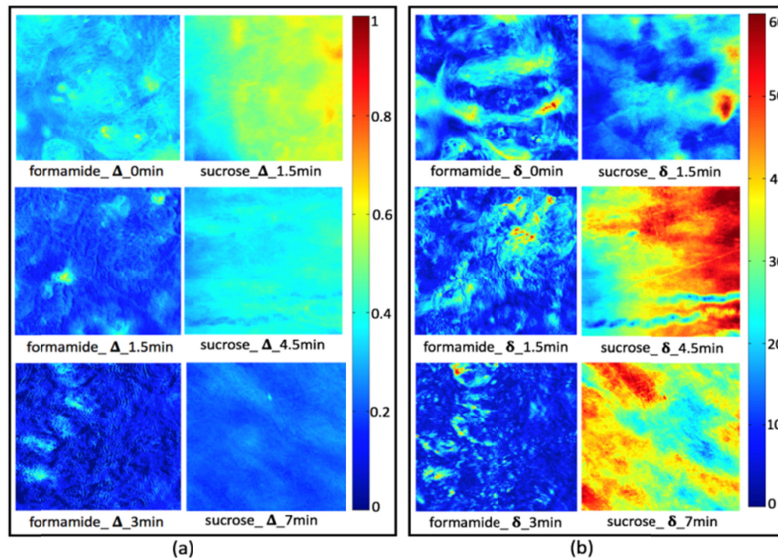

Fig. 6. Pseudo-color images of the MMPD parameter: (a) depolarization parameters Δ and (b) retardation parameter δ for the unstained mouse skin tissue slice.

Combing the Mueller matrix imaging and MMPD parameters from the above experimental figures, we can find out the main polarization features due to clearing and the differences due to different OCAs. In order to speculate what microstructural behavior of tissues have been changed by OCAs and then understand the different clearing mechanisms of two OCAs, next we intend to establish dynamic tissue models corresponding to various possible tissue clearing mechanisms, and then use Monte Carlo simulations of tissue clearing process to verify our hypothesis.
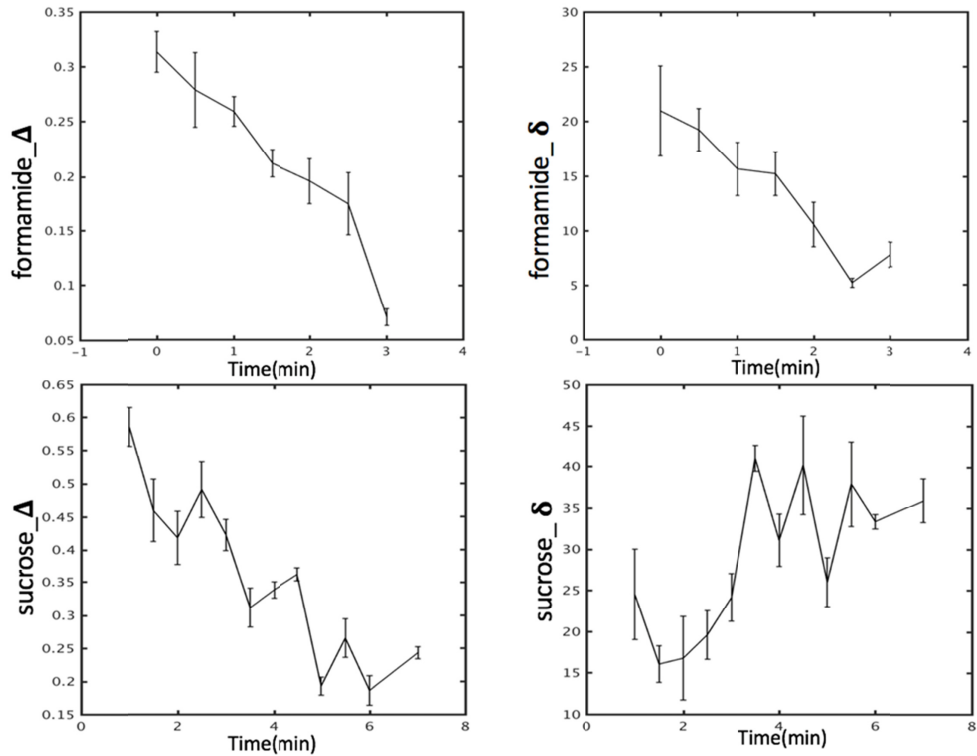

Fig. 7. Experimental values of depolarization and retardation parameter during tissue clearing process using formamide and sucrose as OCAs.

3.2 Monte Carlo simulation of tissue clearing models

In order to understand the key mechanism of the interaction between OCAs and mouse's skin, we mimic the clearing process by setting different dynamic tissue models corresponding to various possible mechanisms. Using Monte Carlo simulation and sphere-cylinder birefringence model (SCBM), the fluctuation of Mueller matrix and MMPD parameters can be deduced. Subsequently, by comparing simulation results with experimental phenomena, we can find out the clearing model that can give the most appropriate explanation of the clearing induced polarization change.

Firstly, we start with the simulation of single mechanism, including refractive index matching, collage shrinkage and more orderly fibers. In the simulation model mimicking refractive index matching, we set a dynamic process of increasing refractive index from 1.35 to 1.40 with an interval of 0.01. In the simulation model mimicking more orderly fibers, the FWHM of the orientation distribution of cylindrical scatterers is reduced from 18 deg to 8 deg with an interval of 2deg. For the case of collagen shrinkage clearing model, we reduce the cylinder diameter step by step from 1.5μm to 0.5μm. Correspondingly, in simulations we have considered the variation of scattering coefficient due to the change of scatterer size and refractive index of intercellular substance.
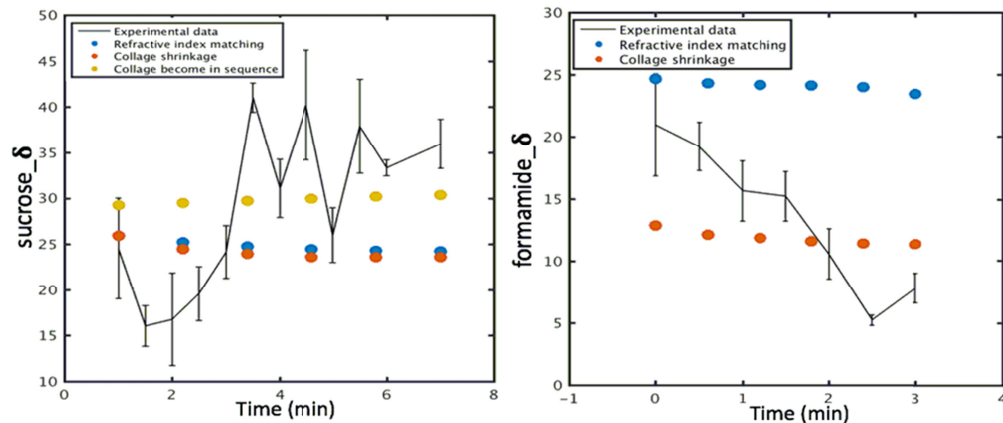
Fig. 8. Comparison of phase retardance between experimental results and Monte Carlo simulations based on one single mechanism models: (a) clearing using sucrose; (b) clearing using formamide.

According to the above experiments, the phase retardance of tissue samples has an opposite trendy with clearing of two kinds of OCAs. Here we investigate the retardance parameter δ firstly. For the case of using saturated sucrose as agent, Fig. 8(a) shows the simulated retardance parameter in three dynamic tissue clearing models, where markers of different colors represent three possible clearing mechanisms respectively. By contrast, the simulated retardance just changes a little, inconsistent with the obvious fluctuation in experiments (solid line in Fig. 8). When using formamide as agent, Fig. 8(b) shows the simulated retardance parameter in two dynamic tissue clearing models. Similarly, the simulations only considering one single mechanism cannot cause an apparent polarization change as experimental phenomena.

Figure 8 implies that the polarization change during tissue clearing of OCAs should be understood by a comprehensive effect of multiple possible mechanisms. In the next simulations, we establish two models to mimic the dynamic influence of formamide: one is refractive index matching plus decreased birefringence; the other is collagen shrinkage plus birefringence reduction. For the case of using saturated sucrose as the agent, we establish three models: refractive index match plus increased birefringence model, collagen shrinkage plus increased birefringence model, and fiber ordering plus increased birefringence model. The simulated MMPD with clearing have been shown in Fig. 9 and can be compared with experimental results marked by solid lines. Compared with single mechanism models, we introduce the variation of birefringence due to the immersion of OCAs into the intercellular substance. The birefringence setting is decreased or increased gradually with an interval of 1e-5.

As shown in Figs. 9(a) and 9(b), both clearing models using formamide can describe the trends of experimental phenomena qualitatively. Relatively speaking, the model including collagen shrinkage seems consistent with the experiments more. From Figs. 9(c) and 9(d), the major polarization variation is the apparent decline of depolarization parameter, Δ, with clearing time. Among three models using saturated sucrose, the one combining refractive index matching and increased birefringence agree with experiments well.
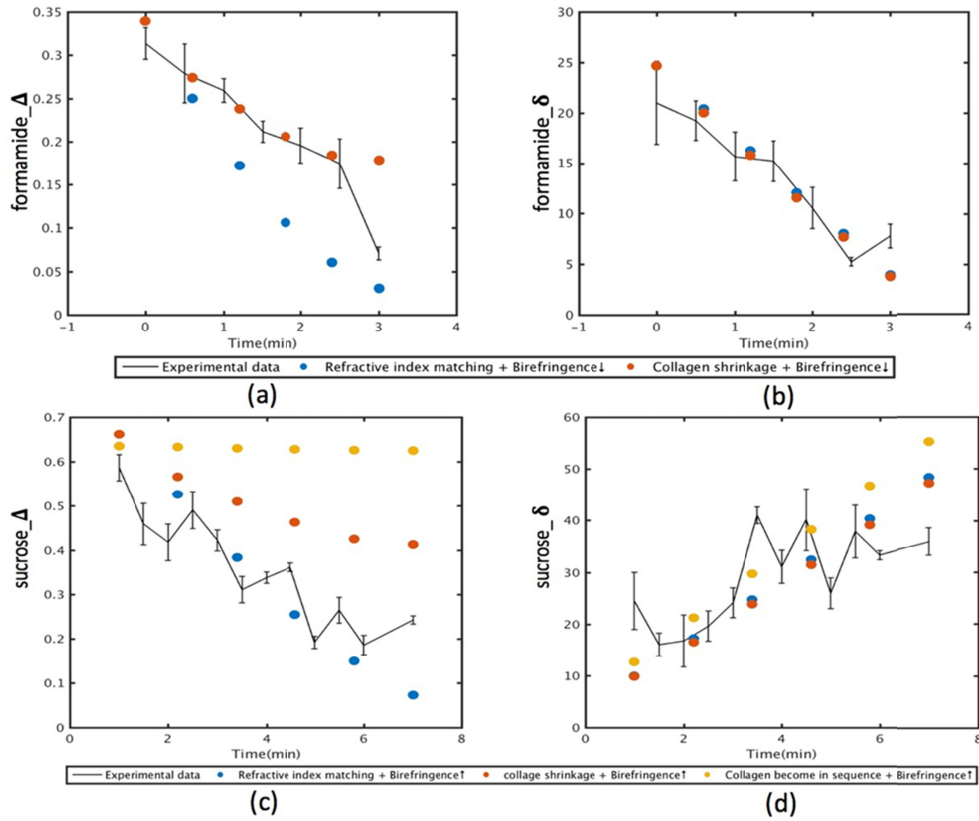
Fig. 9. Comparison of depolarization parameters and retardation parameter between experimental results and Monte Carlo simulations based on multiple mechanism models: (a) **Δ** with clearing using formamide; (b) **δ** with clearing using formamide; (c) **Δ** with clearing using sucrose; (d) **δ** with clearing using sucrose.
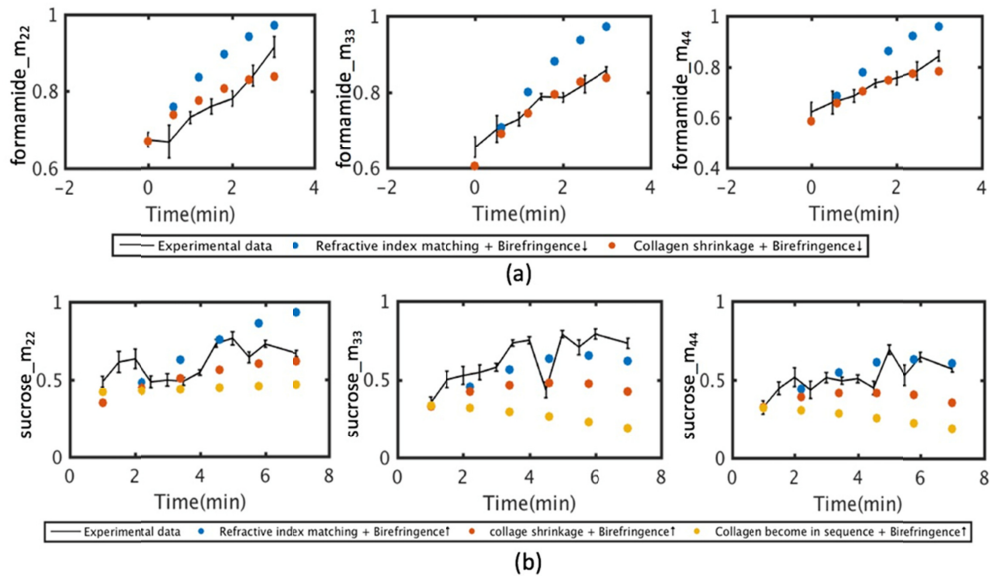

Fig. 10. Monte Carlo simulation results of the three Mueller matrix elements: m22, m33 and m44 using sphere-cylinder birefringence model (SCBM).

According to the above simulations, we can see that a combined model involving multiple mechanisms can better explain the trend of phase retardance with clearing than any single mechanism model. The differences between simulation results of various combined models are the change of depolarization parameter. Then in next simulations we focus on three diagonal elements of Mueller matrix: m22, m33, m44, which are closely related with the depolarization phenomena of measured tissues. Figure 10 shows the simulated diagonal Mueller elements based on different clearing models. By comparing experimental data with simulation results, we can deduce the similar possible clearing models. Specifically, the experimental depolarization parameter,Δ, cannot be close to 1 after formamide clearing (shown in Fig. 10(a)), which supports the model involving collagen shrinkage plus birefringence reduction again. From Fig. 10(b), only the combined model involving refractive index matching and increased birefringence can better mimic the increase of Δ using saturated sucrose as agent than the other two models.

Figures 7, 8, and 9 demonstrate rather regular oscillations of depolarization Δ and retardance δ parameters of the skin during optical clearing at sucrose application. These oscillations for studied nude mouse skin occurred with time-period of approx. 2 min, which is well fit to temporal characteristics of oscillations of optical properties found as 2.5 and 3.5 min for hamster and rat skin at clearing by anhydrous glycerol, respectively [23]. Such quasiperiodic oscillations were described for the first time in Ref [2]. for collagenous tissues like human sclera and then experimentally proved for coherent and polarization (linear parallel- and crossed-polarization) properties of human sclera for which the period of 1.5-2 min was found at application of x-ray contrast trazograph solution [44]. In this paper, it was also hypothesized that the oscillations are the result of temporal-spatially irregular optical clearing agent diffusion driven by a local multi-step dehydration of collagen and dilution of the interstitial fluid. There is a high degree of evidence that a similar mechanism may underlie the temporal oscillatory behavior of the depolarization and retardance parameters.

4. Conclusion

This paper focus on the influence of different clearing agents on polarization features of tissues. By Mueller matrix microscope, we select formamide and saturated sucrose as agents and observe the Mueller matrix images and MMPD change of mouse skin with the clearing time. The differences in experimental phenomena may originate from their respective clearing mechanisms of two kinds of agents. To find out the key factors of making the measured tissue transparent, we consider several possible clearing mechanisms and then establish corresponding single factor models and combined models. We can mimic the dynamic tissue clearing process by simulating the gradual changes of microphysical attributes using our Monte Carlo simulations, and then compare our experimental results with simulations results based on different clearing models.

Firstly, the simulations involving only one mechanism cannot approximate the experimental MMPD, which confirms that tissue clearing is very likely due to multiple mechanisms working together. Further investigation and comparison indicate that different agents have respective influence on the cleared tissue, such as shrinkage due to dehydration, changes in Fiber Orientation and birefringence variation in intercellular substance. Based on the dynamic variations of diagonal Mueller elements, depolarization and phase retardance parameters, this paper try to explain the clearing process by formamide and sucrose. Specifically, tissue clearing by formamide is mainly due to collagen shrinkage plus decreased birefringence, and clearing by saturated sucrose can be mainly due to refractive index matching plus increased birefringence. The investigation including experiments and simulations provides a way to understand the clearing process according to the connection between polarization changes and microphysical features of tissues. In addition, this paper also verify that Mueller matrix imaging is potentially a powerful method applied in tissue clearing.

Disclosures

The authors declare that there are no conflicts of interest related to this article.

References

1. D. S. Richardson and J. W. Lichtman, "Clarifying tissue clearing," Cell **162**(2), 246–257 (2015).
2. V. V. Tuchin, I. L. Maksimova, D. A. Zimnyakov, I. L. Kon, A. H. Mavlyutov, and A. A. Mishin, "Light propagation in tissues with controlled optical properties," J. Biomed. Opt. **2**(4), 401–417 (1997).
3. M. T. Ke, Y. Nakai, S. Fujimoto, R. Takayama, S. Yoshida, T. S. Kitajima, M. Sato, and T. Imai, "Super-resolution mapping of neuronal circuitry with an index-optimized clearing agent," Cell Reports **14**(11), 2718–2732 (2016).
4. W. Feng, R. Shi, N. Ma, D. K. Tuchina, V. V. Tuchin, and D. Zhu, "Skin optical clearing potential of disaccharides," J. Biomed. Opt. **21**(8), 081207 (2016).
5. L. Silvestri, I. Costantini, L. Sacconi, and F. S. Pavone, "Clearing of fixed tissue: a review from a microscopist's perspective," J. Biomed. Opt. **21**(8), 081205 (2016).
6. K. Tainaka, A. Kuno, S. I. Kubota, T. Murakami, and H. R. Ueda, "Chemical principles in tissue clearing and staining protocols for whole-body cell profiling," Annu. Rev. Cell Dev. Biol. **32**(1), 713–741 (2016).
7. K. H. R. Jensen and R. W. Berg, "Advances and perspectives in tissue clearing using CLARITY," J. Chem. Neuroanat. **86**, 19–34 (2017).
8. T. Yu, J. Zhu, Y. Li, Y. Ma, J. Wang, X. Cheng, S. Jin, Q. Sun, X. Li, H. Gong, Q. Luo, F. Xu, S. Zhao, and D. Zhu, "RTF: a rapid and versatile tissue optical clearing method," Sci. Rep. **8**(1), 1964 (2018).
9. P. Wan, J. Zhu, J. Xu, Y. Li, T. Yu, and D. Zhu, "Evaluation of seven optical clearing methods in mouse brain," Neurophotonics **5**(3), 035007 (2018).
10. D. Zhu, K. V. Larin, Q. Luo, and V. V. Tuchin, "Recent progress in tissue optical clearing," Laser Photonics Rev. **7**(5), 732–757 (2013).
11. K. V. Larin, M. G. Ghosn, A. N. Bashkatov, E. A. Genina, N. A. Trunina, and V. V. Tuchin, "Optical clearing for OCT image enhancement and in-depth monitoring of molecular diffusion," IEEE J. Sel. Top. Quantum Electron. **18**(3), 1244–1259 (2012).
12. R. Shi, M. Chen, V. V. Tuchin, and D. Zhu, "Accessing to arteriovenous blood flow dynamics response using combined laser speckle contrast imaging and skin optical clearing," Biomed. Opt. Express **6**(6), 1977–1989 (2015).
13. Y.-Y. Fu and S.-C. Tang, "Optical clearing facilitates integrated 3D visualization of mouse ileal microstructure and vascular network with high definition," Microvasc. Res. **80**(3), 512–521 (2010).
14. O. Nadiarnykh and P. J. Campagnola, "Retention of polarization signatures in SHG microscopy of scattering tissues through optical clearing," Opt. Express **17**(7), 5794–5806 (2009).
15. O. Nadiarnykh and P. J. Campagnola, SHG and optical clearing, in *Second Harmonic Generation Imaging*, F. S. Pavone, P. J. Campagnola, eds.(CRC Press, 2014), pp. 169–189.
16. P. S. Tsai, J. P. Kaufhold, P. Blinder, B. Friedman, P. J. Drew, H. J. Karten, P. D. Lyden, and D. Kleinfeld, "Correlations of neuronal and microvascular densities in murine cortex revealed by direct counting and colocalization of nuclei and vessels," J. Neurosci. **29**(46), 14553–14570 (2009).
17. I. Costantini, J. P. Ghobril, A. P. Di Giovanna, A. L. Allegra Mascaro, L. Silvestri, M. C. Müllenbroich, L. Onofri, V. Conti, F. Vanzi, L. Sacconi, R. Guerrini, H. Markram, G. Iannello, and F. S. Pavone, "A versatile clearing agent for multi-modal brain imaging," Sci. Rep. **5**(1), 9808 (2015).
18. I. V. Meglinski, D. Y. Churmakov, A. N. Bashkatov, E. A. Genina, and V. V. Tuchin, "The Enhancement of Confocal Images of Tissues at Bulk Optical Immersion," Laser Phys. **13**(1), 65–69 (2004).
19. T. Kuwajima, A. A. Sitko, P. Bhansali, C. Jurgens, W. Guido, and C. Mason, "ClearT: a detergent- and solvent-free clearing method for neuronal and non-neuronal tissue," Development **140**(6), 1364–1368 (2013).
20. T. Yu, Y. Qi, J. Wang, W. Feng, J. Xu, J. Zhu, Y. Yao, H. Gong, Q. Luo, and D. Zhu, "Rapid and prodium iodide-compatible optical clearing method for brain tissue based on sugar/sugar-alcohol," J. Biomed. Opt. **21**(8), 081203 (2016).
21. A. Y. Sdobnov, M. E. Darvin, E. A. Genina, A. N. Bashkatov, J. Lademann, and V. V. Tuchin, "Recent progress in tissue optical clearing for spectroscopic application," Spectrochim. Acta A Mol. Biomol. Spectrosc. **197**, 216–229 (2018).
22. W. R. Lee, R. Y. Tsai, C. L. Fang, C. J. Liu, C. H. Hu, and J. Y. Fang, "Microdermabrasion as a novel tool to enhance drug delivery via the skin: an animal study," Dermatol. Surg. **32**(8), 1013–1022 (2006).
23. O. F. Stumpp, A. J. Welch, T. E. Milner, and J. Neev, "Enhancement of transepidermal skin clearing agent delivery using a 980 nm diode laser," Lasers Surg. Med. **37**(4), 278–285 (2005).

24. A. K. Nugroho, G. L. Li, M. Danhof, and J. A. Bouwstra, "Transdermal iontophoresis of rotigotine across human stratum corneum in vitro: influence of pH and NaCl concentration," Pharm. Res. **21**(5), 844–850 (2004).
25. A. Tezel and S. Mitragotri, "Interactions of inertial cavitation bubbles with stratum corneum lipid bilayers during low-frequency sonophoresis," Biophys. J. **85**(6), 3502–3512 (2003).
26. V. V. Tuchin, G. B. Altshuler, A. A. Gavrilova, A. B. Pravdin, D. Tabatadze, J. Childs, and I. V. Yaroslavsky, "Optical clearing of skin using flash lamp-induced enhancement of epidermal permeability," Lasers Surg. Med. **38**(9), 824–836 (2006).
27. S. Carvalho, N. Gueiral, E. Nogueira, R. Henrique, L. Oliveira, and V. V. Tuchin, "Glucose diffusion in colorectal mucosa-a comparative study between normal and cancer tissues," J. Biomed. Opt. **22**(9), 91506 (2017).
28. E. A. Genina, A. N. Bashkatov, and V. V. Tuchin, "Tissue optical immersion clearing," Expert Rev. Med. Devices **7**(6), 825–842 (2010).
29. V. V. Tuchin, "Polarized light interaction with tissues," J. Biomed. Opt. **21**(7), 71114 (2016).
30. B. Kunnen, C. Macdonald, A. Doronin, S. Jacques, M. Eccles, and I. Meglinski, "Application of circularly polarized light for non-invasive diagnosis of cancerous tissues and turbid tissue-like scattering media," J. Biophotonics **8**(4), 317–323 (2015).
31. Y. Wang, H. He, J. Chang, N. Zeng, S. Liu, M. Li, and H. Ma, "Differentiating characteristic microstructural features of cancerous tissues using Mueller matrix microscope," Micron **79**, 8–15 (2015).
32. M. Sun, H. He, N. Zeng, E. Du, Y. Guo, S. Liu, J. Wu, Y. He, and H. Ma, "Characterizing the microstructures of biological tissues using Mueller matrix and transformed polarization parameters," Biomed. Opt. Express **5**(12), 4223–4234 (2014).
33. C. He, H. He, X. Li, J. Chang, Y. Wang, S. Liu, N. Zeng, Y. He, and H. Ma, "Quantitatively differentiating microstructures of tissues by frequency distributions of Mueller matrix images," J. Biomed. Opt. **20**(10), 105009 (2015).
34. S. Alali and A. Vitkin, "Polarized light imaging in biomedicine: emerging Mueller matrix methodologies for bulk tissue assessment," J. Biomed. Opt. **20**(6), 61104 (2015).
35. J. Qi and D. S. Elson, "Mueller polarimetric imaging for surgical and diagnostic applications: a review," J. Biophotonics **10**(8), 950–982 (2017).
36. E. Du, H. He, N. Zeng, Y. Guo, R. Liao, Y. He, and H. Ma, "Two-dimensional backscattering Mueller matrix of sphere-cylinder birefringence media," J. Biomed. Opt. **17**(12), 126016 (2012).
37. D. Chen, N. Zeng, Y. Wang, H. He, V. V. Tuchin, and H. Ma, "Study of optical clearing in polarization measurements by Monte Carlo simulations with anisotropic tissue-mimicking models," J. Biomed. Opt. **21**(8), 081209 (2016).
38. D. Chen, N. Zeng, Q. Xie, H. He, V. V. Tuchin, and H. Ma, "Mueller matrix polarimetry for characterizing microstructural variation of nude mouse skin during tissue optical clearing," Biomed. Opt. Express **8**(8), 3559–3570 (2017).
39. T. Yun, N. Zeng, W. Li, D. Li, X. Jiang, and H. Ma, "Monte Carlo simulation of polarized photon scattering in anisotropic media," Opt. Express **17**(19), 16590–16602 (2009).
40. H. He, N. Zeng, R. Liao, T. Yun, W. Li, Y. He, and H. Ma, "Application of sphere-cylinder scattering model to skeletal muscle," Opt. Express **18**(14), 15104–15112 (2010).
41. Y. Dong, H. He, W. Sheng, J. Wu, and H. Ma, "A quantitative and non-contact technique to characterise microstructural variations of skin tissues during photo-damaging process based on Mueller matrix polarimetry," Sci. Rep. **7**(1), 14702 (2017).
42. A. N. Bashkatov, E. A. Genina, and V. V. Tuchin, "Optical properties of skin, subcutaneous and muscle tissue: A review," J. Innov. Opt. Health Sci. **4**(1), 9–38 (2011).
43. A. N. Bashkatov, E. A. Genina, V. I. Kochubey, and V. V. Tuchin, "Optical properties of human skin, subcutaneous and mucous tissues in the wavelength range from 400 to 2000 nm," J. Phys. D Appl. Phys. **38**(15), 2543–2555 (2005).
44. V. V. Tuchin, "Coherent optical techniques for the analysis of tissue structure and dynamics," J. Biomed. Opt. **4**(1), 106–124 (1999).